ACS OMEGA

Open Access

http://pubs.acs.org/journal/acsodf

Article

Zinc–Carbon Battery Recycling for Investigating Carbon Materials for Supercapacitor Applications

Thuy Trang T. Vuong, Phi Long Nguyen, Nghia Trong Nguyen,* Thi Viet Bac Phung,* and Phuoc-Anh Le

Cite This: *ACS Omega* 2024, 9, 22543−22556

Read Online

ACCESS | Metrics & More | Article Recommendations | Supporting Information

ABSTRACT: In this paper, carbon materials, including graphene nanosheets and carbon nanoparticles, were prepared from spent zinc−carbon batteries by the following two simple methods: electrochemical exfoliation and ultrasonication. Here, graphene nanosheets were synthesized by electrochemical exfoliation in 0.5 M H_2SO_4 by using a direct current power supply with two carbon rods from spent zinc−carbon batteries. Carbon nanoparticles were prepared by fast ultrasonication in a low-cost, green solution of DI water and ethanol. Graphene nanosheets in this study have high quality, large scale, and good electrochemical ability, while carbon nanoparticles have a unique nanosize and a good specific surface area. These carbon materials were applied for electrochemical measurements for supercapacitor studies and showed excellent stability at different temperatures. Moreover, electric double-layer capacitor devices based on graphene nanosheets and carbon nanoparticles were also used in electrochemical studies with strong stability and good electrochemical capability.

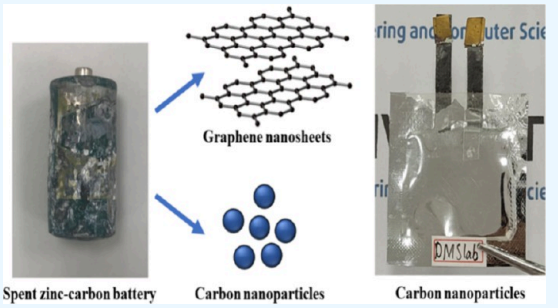

1. INTRODUCTION

The rapid growth of the global economy has significantly increased the use of fossil fuels, a fuel source that is inherently limited in resources and has environmental impacts, such as global warming, environmental pollution, and climate change. To minimize the use of fossil fuel sources, scientific researchers around the world have been searching for different energy sources that can replace this fuel source in the near future.[1,2] The effective use of energy sources and the search for renewable energy sources are extremely urgent.[2,3] Over the past decade, the use of renewable energy has increased significantly, leading to a rapid increase in the renewable energy capacity. This has motivated the search for suitable renewable energy storage sources to accommodate the increase in capacity of such renewable energy sources.[4,5] Therefore, high-performance, environmentally friendly renewable energy storage technologies are an effective solution for clean and renewable energy sources.[6]

The disposal of spent batteries into the environment is an alarming problem because various types of heavy metals can disperse into the environment to pollute groundwater, then enter fish and crops, destroy the survival environment, and indirectly threaten human health. Nowadays, battery usage is increasing, leading to an increase in spent batteries, but not everyone knows how to handle them. Therefore, a battery recycling strategy is a great way to help protect the environment.[7,8] There are many different types of batteries, and they are classified based on their composition. Consequently, each type of battery will come with different material recycling processes.[9,10] Battery recycling refers to the method of reusing and reprocessing batteries to reduce the number of batteries discarded as waste. Recycling can assist in extracting raw components from spent batteries and sending them to product manufacturing businesses for reuse.[11] Among various battery types, zinc−carbon batteries are the first commercial dry batteries and are widely used because they provide high energy density and good durability and are very low-cost. Thus, they are common in every home, leading to an extremely large amount of batteries being released into the environment.[12−14] The construction of a zinc−carbon battery consists of a graphite rod surrounded by carbon powder and encased by a zinc casing with an electrolyte of ammonium chloride.[15] The components in zinc−carbon batteries are not environmentally friendly and have large emissions, so they need to be collected and recycled properly to avoid polluting the environment.[16,17] Here, we refer to the recycling of zinc−carbon batteries by electrochemical exfoliation and ultrasonication methods to avoid wasting fuel resources and not polluting the environment. This research involves simple and

Received: October 28, 2023
Revised: April 25, 2024
Accepted: April 30, 2024
Published: May 15, 2024

effective strategies to synthesize graphene and carbon nanoparticle materials for supercapacitor electrodes.

Supercapacitors (SCs) are a developing technology that attracts a lot of attention from researchers because they have flexible power sources, high specific capacity, high energy density, long cycle life, high efficiency, environmental friendliness, high safety, and fast charging and discharging speeds.[18−20] SCs are devices that can store large amounts of electrical energy and release it quickly, making them ideal for use in a wide range of applications.[21−23] The performance and endurance of energy storage devices, such as batteries and supercapacitors, are significantly influenced by the material used for the electrodes.[24,25,26] As a result, the two primary kinds of carbon materials that are the subject of this study are carbon nanoparticles and graphene nanosheets, which are, respectively, two-dimensional and zero-dimensional electrode materials. Hence, the goal of developing a low-cost energy storage device that satisfies the majority of the essential requirements of the electric double-layer capacitor type's essential requirements.

In this research, graphene nanosheets and carbon nanoparticle materials were collected and recycled from spent zinc−carbon batteries synthesized by electrochemical exfoliation and simple ultrasonic treatment for application as electrode materials for symmetrical solid-state supercapacitors (SSCs). The structure, morphology, and electrochemical properties of the above recycled materials were determined by various techniques to provide interesting ideas for battery recycling.

2. EXPERIMENTAL SECTION

2.1. Materials. Spent zinc−carbon batteries were collected from the supermarket. Charcoal activated powder (AR) was purchased from the Damao chemical reagent factory. Sodium sulfate (Na_2SO_4) was purchased from Sigma-Aldrich. Sulfuric acid (H_2SO_4, 95%) was bought from Samchun Chemical Co., Ltd.; *N*-methyl-2-pyrrolidone (NMP); and N−N-dimethylformamide (DMF) were purchased from Shanghai Zhanyun Chemical Co., Ltd. Polyvinylidene difluoride (PVDF) and poly(vinyl alcohol) (PVA) were produced from Aladdin and Macklin, respectively.

2.2. Graphene Nanosheets and Carbon Nanoparticles' Preparation. Graphene nanosheets were synthesized by a one-step electrochemical exfoliation. First, two carbon rods from spent zinc−carbon batteries were immersed in 0.5 M H_2SO_4 under an applied voltage of 4.5 V for 24 h. Then, the final mixture was collected, filtrated, and dried at 80 °C for 24 h to obtain graphene nanosheets.

Carbon nanoparticles were prepared by fast ultrasonic processing. The solution of 200 mg of carbon powder from the spent zinc−carbon batteries was mixed with 200 mL of ethanol and isopropyl alcohol (ratio 1:1) with ultrasonication for 6 h. Then, this final mixture was filtrated, washed several times, and dried at 80 °C for 24 h to obtain carbon nanoparticles.

2.3. Material Characterizations. Graphene nanosheets and carbon nanoparticle morphology and structure were studied by the following various different measurements: X-ray diffraction (XRD, Bruker D2, Cu Kα tube), Raman spectroscopy (Jobin won, Horiba, Ar laser source with an excitation wavelength of 520 nm), scanning electron microscopy (SEM, Hitachi SU8000 and JEOL, JSM-IT800), and transmission electron microscopy (TEM, JEM-ARM200F).

The graphene nanosheet (G) and carbon nanoparticle (C_{NPs}) electrodes were prepared by following the solution mixing method. First, 80 mg of active materials (graphene nanosheets or carbon nanoparticles; 80 wt %), 10 mg of charcoal (10 wt %), and 10 mg of PVDF (10 wt %) were mixed together in 3 mL of NMP with constant stirring at 80 °C and reduced to 27 °C for 3 days to obtain homogeneous slurries. Then, 30 μL of these slurries was coated on a carbon paper substrate over an area of 1.5 × 1.5 cm (~2.25 cm^2) and then dried at 80 °C under a vacuum environment for 3 days to obtain graphene electrodes with 1 mg of each electrode.

The three-electrode system used G or C_{NPs} as the working electrode, Pt foil as the counter electrode, Ag/AgCl as the reference electrode, and 1 M Na_2SO_4 as the aqueous electrolyte. The supercapacitor devices in this report used a gel polymer electrolyte system of PVA-Na_2SO_4. This gel polymer electrolyte was prepared by the solution-mixing method. Here, 300 mg of PVA (30 wt %), 700 mg of Na_2SO_4 (70 wt %), and 20 mL of DI water were mixed together with constant stirring at 100 °C for 30 min to obtain a clear gel polymer electrolyte solution.

The symmetrical solid-state supercapacitors (SSCs) were fabricated by following the sandwich structure: electrode/PVA-Na_2SO_4/electrode. Two electrodes were immersed in the (PVA-Na_2SO_4) gel polymer electrolyte and dried in the air. Then, one piece (4 cm^2) of oil absorbent paper was immersed in gel polymer electrolyte, and they were fabricated into pouch cell types.

The electrochemical studies of the supercapacitors were studied on an electrochemical workstation CS310 (Corrtest, China) by following various techniques, including cyclic voltammetry (CV), electrochemical impedance spectroscopy (EIS), and galvanostatic charge−discharge (GCD).

The specific capacitance of the supercapacitor (C, F g^{-1}) and the symmetrical supercapacitor devices (C_s, F g^{-1}) were calculated from the charge−discharge curve using the following equations:[9,27]

$$C = \frac{I \times \Delta t}{\Delta V \times m} \tag{1}$$

$$C_s = 4C \tag{2}$$

The energy density (E, W h kg^{-1}) and power density (P, W kg^{-1}) were calculated by the following equations:[9,27]

$$E = \frac{C_i \times (\Delta V)^2}{2} \times \frac{1000}{3600} \tag{3}$$

$$P = \frac{E \times 3600}{\Delta t} \tag{4}$$

where I (A) is the current, Δt (s) is the discharge time, $\Delta V = (V_2 - V_1)$ (V) is the working voltage window, m (g) is the total mass volume of the electrode material, C_i (F g^{-1}) is the specific capacitance of the working electrode in a three-electrode system (C) or devices (C_S).

Moreover, the specific capacitance (C_{CV}, F g^{-1}) could also be calculated based on CV curves:[9,27]

$$C_{CV} = \frac{\int I dV}{2 \times (V_2 - V_1) \times m \times v} \tag{5}$$

where v is the scan rate (V s^{-1}).

https://doi.org/10.1021/acsomega.3c08537
ACS Omega 2024, 9, 22543−22556

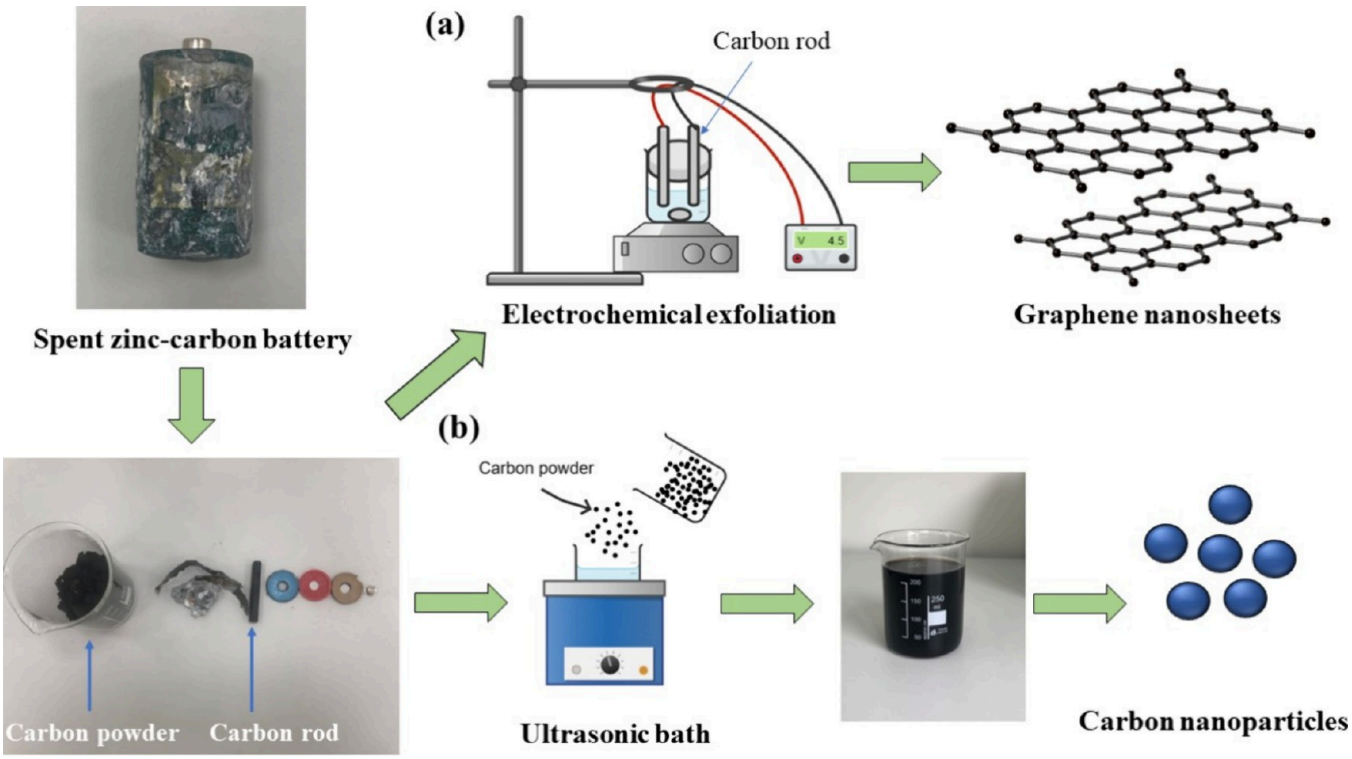

Figure 1. (a) Graphene nanosheets' preparation by electrochemical exfoliation and (b) carbon nanoparticles' preparation by ultrasonication.

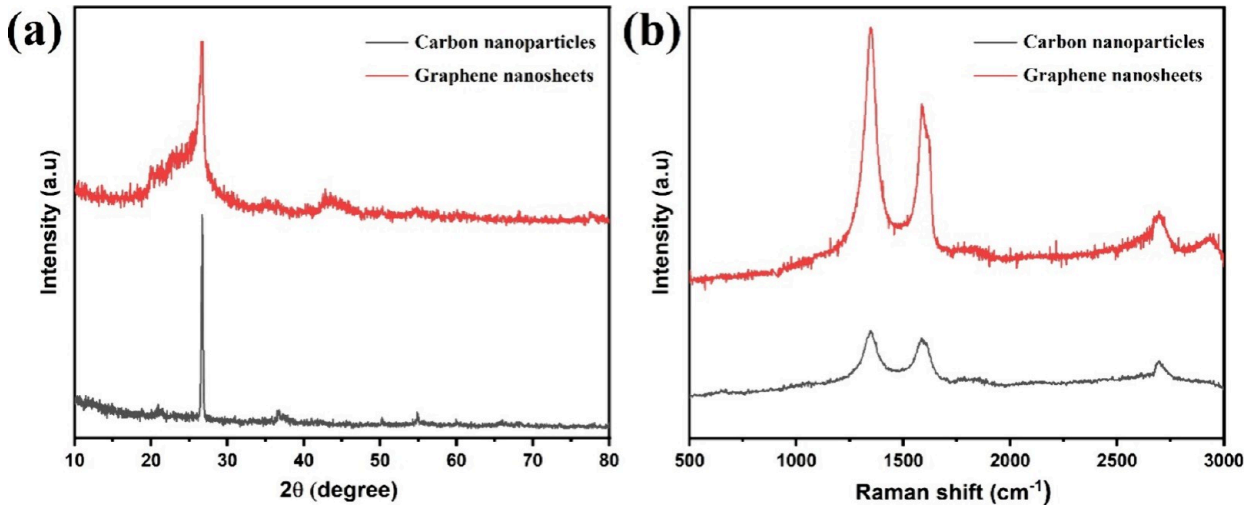

Figure 2. (a) XRD pattern and (b) Raman spectroscopy of graphene nanosheets and carbon nanoparticles.

The Coulombic efficiency was calculated from the GCD curves by the following equation:[9,27]

$$\varepsilon = \frac{t_{\text{discharge}}}{t_{\text{charge}}} \times 100\% \quad (6)$$

where $t_{\text{discharge}}$ is the discharge time, while t_{charge} is the charge time

3. RESULTS AND DISCUSSION

Figure 1a shows the exfoliation process to prepare graphene nanosheets in a 0.5 M H_2SO_4 electrolyte with two carbon rod electrodes that were collected from spent batteries. When a direct current (DC) voltage of +4.5 V was applied to the two carbon rod electrodes, the positive carbon rod began to dissociate and disperse into the electrolyte solution. Through filtration and vacuum firing, powdered graphene nanosheets are obtained. While carbon nanoparticles were obtained from spent zinc−carbon batteries, they were then ultrasonically vibrated, filtered, and vacuum-heated several times to obtain the final product (Figure 1b). Here, spent zinc−carbon batteries are recycled and applied to supercapacitor applications, and fully utilizing the components in them will provide a promising way to protect the environment.

3.1. Morphological and Structural Features. The morphological characterization of graphene nanosheets and carbon nanoparticles was carried out by XRD and Raman measurements via powder sample preparations. Figure 2a shows the XRD patterns of the graphene nanosheets and carbon nanoparticles. The highest diffraction peak at position

https://doi.org/10.1021/acsomega.3c08537
ACS Omega 2024, 9, 22543−22556

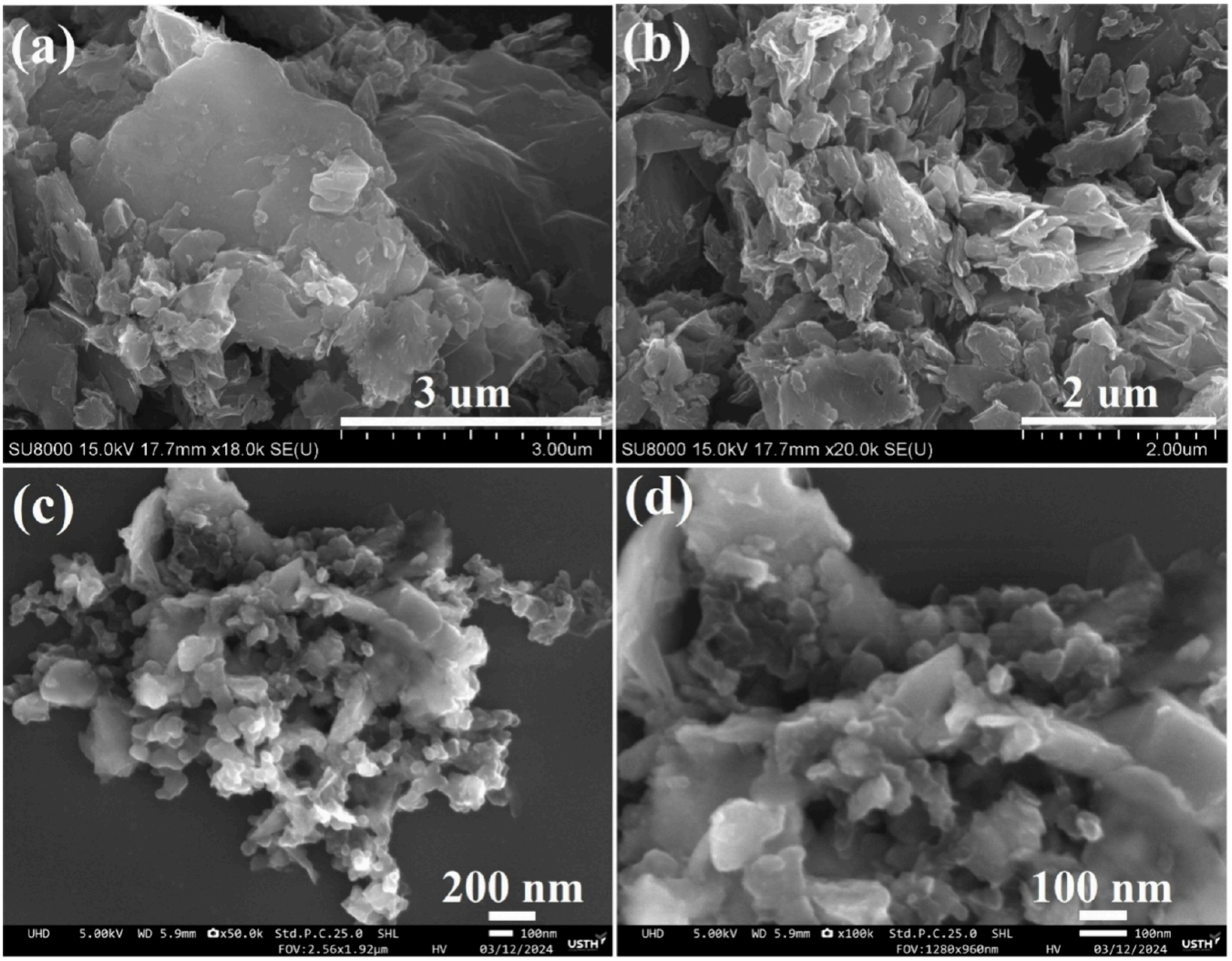

Figure 3. SEM images of (a, b) graphene nanosheets and (c, d) carbon nanoparticles.

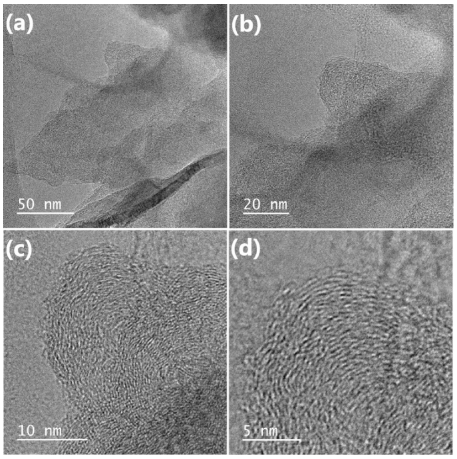

Figure 4. (a–d) TEM images of graphene nanosheets at various magnifications.

$2\theta = 26.57°$ is attributed to (002) and $2\theta = 43.2°$ is assigned to (100), which is equivalent to graphene nanosheets and carbon nanoparticles with disordered structures.[28,29] Because both of these samples are made of carbon material, the XRD spectra are similar. However, the strong peak of graphene nanosheet powder has a very high intensity due to its high crystallinity, while the broad and weak peak of carbon nanoparticles indicates a low crystal phase corresponding to low-crystal nanoparticles by the SEM measurement. Moreover, the high strength of the peak at position $2\theta = 26.57°$ indicates that the high concentration of the crystal phase in the material is consistent with the TEM result. For a better understanding of the structure of graphene nanosheets and carbon nanoparticles, we conducted Raman scattering measurements. In Figure 2b, it is clear that the two peaks are located at about 1347.01 cm^{-1} (the D band) and 1585.84 cm^{-1} (the G band). The D band is associated with a disturbed graphite structure defect, and the G band corresponds to the 2D graphite network vibration mode.[30] These results demonstrate relatively stable conductivity due to the high crystalline phase in graphene nanosheets and carbon nanoparticles.

Figure 3 shows SEM images of graphene nanosheets and carbon nanoparticles. Figure 3a,b shows the characteristic wrinkles and folds of the created graphene nanosheets. It confirms that 2D graphene nanosheets can be produced using the exfoliation method. Observing the SEM image, it can be seen that the size of the graphene nanosheets obtained is up to several micrometers. Figure 3c,d shows the carbon nanoparticles clustered together, exhibiting a relatively uniform

https://doi.org/10.1021/acsomega.3c08537
ACS Omega 2024, 9, 22543−22556

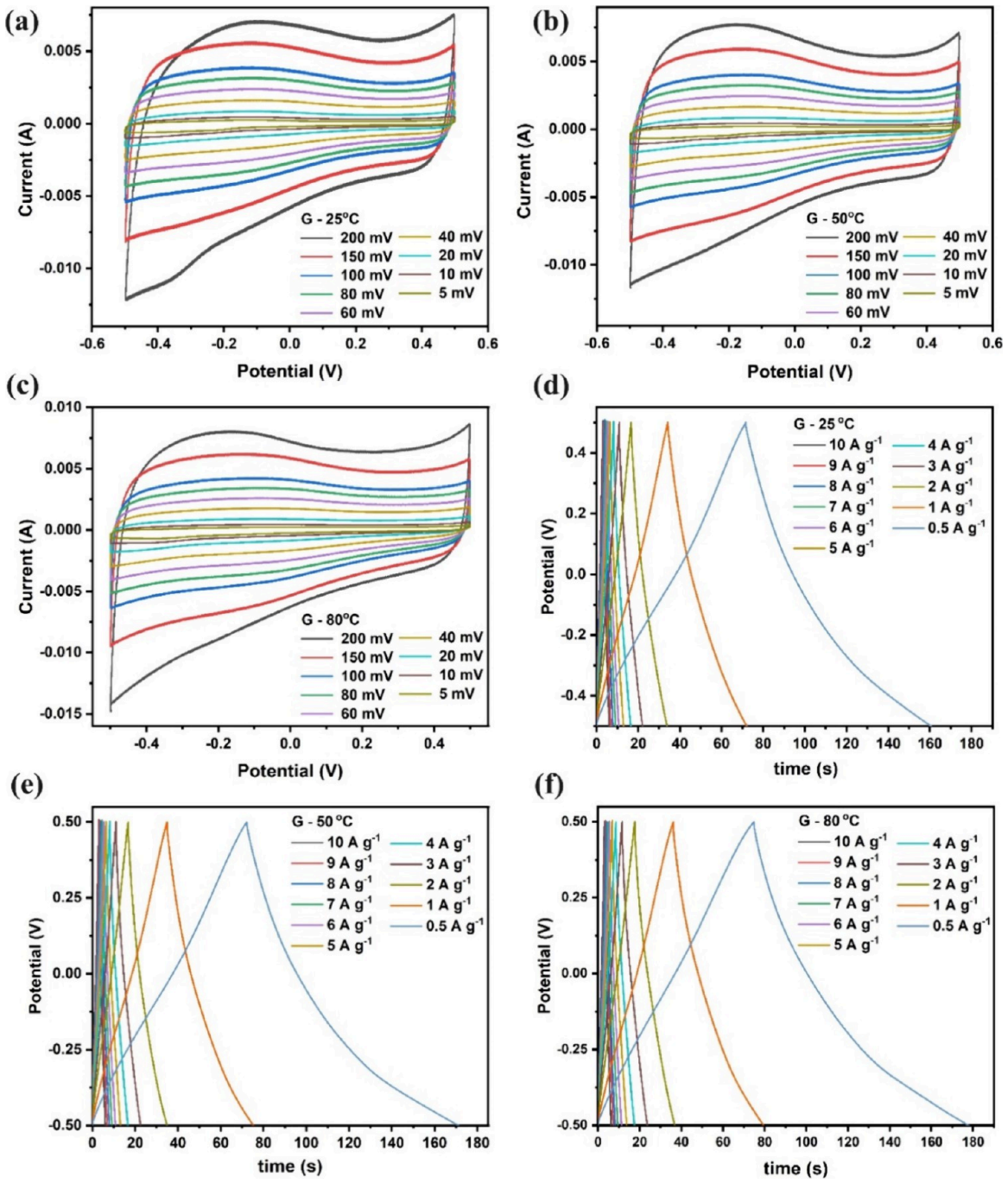

Figure 5. Electrochemical studies of a three-electrode system for G electrodes: (a−c) CV curves and (d−f) GCD curves at 25, 50, and 80 °C, respectively.

spherical structure and an average particle size of about 50 nm. Through the methods of ultrasonic vibration, filtration, and calcination in vacuum, carbon nanoparticles can be obtained relatively effectively. SEM pictures further show that the carbon layer changed from a naturally occurring ordered lamellar arrangement to an asymmetric structure with varying diameters and a rough, discontinuous layered appearance. This occurs because the material's structure changes as it passes through a liquid medium, causing oxidation and expansion during the electrochemical exfoliation process. It may also be connected to the washing, filtering, and drying processes.

To demonstrate the feasibility, quality, and yield of graphene electrolyzed in a 1 M H_2SO_4 solution through two electrode rods taken from zinc batteries, the TEM image of graphene has been shown in Figure 4. TEM images of graphene in Figure 4a,b show the 2D structural morphological properties of the material. At higher resolutions (Figure 4c,d), thin layers of graphene can be seen stacked on top of each other, forming veins. Here, the graphene nanosheet was only piled into a few layers; thus, it is visible to be transparent under the TEM, and the graphene contour is clearly visible in the picture. One of the common characteristics of graphene is its wrinkled edges, and the tiny columnar area might be a dispersant. Moreover, the layers of highly dispersible sheets are maintained in the graphene nanosheets of oxide by the presence of groups with hydrophilic functionality, such as COC, C═O, COOH, and

https://doi.org/10.1021/acsomega.3c08537
ACS Omega 2024, 9, 22543−22556

Table 1. Coulombic Efficiency of Graphene Nanosheets and Carbon Nanoparticles' Working Electrodes

	G working electrode			C_{NPs} working electrode		
current density (A g^{-1})	$\varepsilon_{25\ °C}$ (%)	$\varepsilon_{50\ °C}$ (%)	$\varepsilon_{80\ °C}$ (%)	$\varepsilon_{25\ °C}$ (%)	$\varepsilon_{50\ °C}$ (%)	$\varepsilon_{80\ °C}$ (%)
10	100	101	104.3	150	133.3	122.2
9	100	100	101.9	127.3	125	108.3
8	101.7	101.7	104.2	106.6	126.7	106.2
7	100.7	101.5	102.9	122	114.3	110
6	101.3	101.2	103	111.5	114.8	107.7
5	102	102	103.4	111.4	110	105.4
4	102	102.8	103.9	111.8	108.7	105.6
3	102.7	104.5	105.5	112	111	108
2	105	108.4	109.3	115.5	113.3	109.6
1	110.7	116.2	119.9	117.1	119	117
0.5	123.7	137.2	137.8	128.9	134.2	141.5

OH. This offers greater attraction for usage in polymer composites, sustainable energy conversion, electronics applications, and storage.

3.2. Electrochemical Properties. *3.2.1. Electrochemical Studies of a Three-Electrode System.* The electrochemical properties of graphene nanosheets (G) and carbon nanoparticle (C_{NPs}) electrodes were studied according to the three-electrode measurement method, and the symmetrical solid-state supercapacitors were assembled for characterization. Here, these materials provide the promising electrochemical capability of an electric double-layer capacitor. When current flows through the electrodes, the ions will be separated and diffused into the opposite electrode (negative ions will move to the anode, positive ions will move to the cathode) and form two electrostatic layers on either side. Figure 5 shows the CV and GCD curves of the G electrode at various different temperatures of 25, 50, and 80 °C, respectively, at different scanning rates and current densities. The material has an applied voltage from −0.5 to 0.5 V. Figure 5a,b,c depicts the CV curves of the G electrode at 25, 50, and 80 °C. The CV curves show a roughly rectangular shape and a change in current intensity between different scan rates, varying in descending order, corresponding to scan rates from 200 to 5 mV.[31] CV curves that closely resemble a rectangle indicate good storage capacity, which makes them ideal for supercapacitor devices.[9,32,33] When the electrodes are scanned at a high current scanning rate, the G electrode in the electrolyte solution will be affected by higher diffusion resistance and greater electrochemical polarization, which, in turn, affects the characteristics of the capacitor and the interaction between the G electrode and the electrolyte solution. The GCD curves in Figure 5d−f illustrate shapes close to triangles, indicating efficient ion transport through the stable electrode. Furthermore, at different current densities from 10 to 0.5 A g^{-1}, the GCD curves showed linearity with stable discharge reversibility of the G electrode.[31,32,34] The Coulumbic efficiency of the G electrode at various current densities from 10 to 0.5 A g^{-1} is quite balanced (Table 1), which indicates excellent ion transportation during the charge−discharge process.

To further survey the ion transport and internal impedance of the electrodes, EIS measurements were investigated. As shown in Figure 6a, the EIS results of the G electrode are in the range of 100 mHz to 100 kHz with an applied amplitude of 5 mV. The linear slope of the Nyquist plots in the low-frequency region confirms the mass transfer process.[35,36] This indicates faster diffusion of ions in the electrolyte. The relatively equivalent series resistances of EIS measurements of supercapacitors illustrate the good conductivity and ion transfer at the electrode/electrolyte interface.[37,38] The equivalent series resistances of the samples measured at different temperatures of 25, 50, and 80 °C are 1.41, 1.15, and 0.9 Ω, respectively. Here, equivalent series resistances include the resistance of the electrode to the electrolyte, the intrinsic resistance of the electrode, and the resistance of the 1 M Na_2SO_4 electrolyte, which is illustrated by following the corresponding Randles circuit in Figure S1a. As shown in Figure 6b,c, it can be clearly seen that the CV curves and GCD curves of sample G at different temperatures almost coincide with each other at the same scan rate of 5 mV and a density current of 0.5 A g^{-1}. This also proves that the G electrode has durability at high temperatures. Moreover, the specific capacitance of the working electrode in Figure 6f can be calculated from CV curves based on eq 5, where the highest values of 5 mV s^{-1} are 44.03, 45.3, and 48.55 F g^{-1} at different temperatures of 25, 50, and 80 °C, respectively. To research the electrochemical performance of the electrodes, the specific capacitance of the electrodes at different current densities was calculated through GCD curves based on eqs 1, 3, 4 and is shown specifically in Figure 6d. The maximum specific capacitance of graphene samples at different temperatures of 25, 50, and 80 °C delivered values of 44.25, 49.52, and 51.53 F g^{-1}, respectively, at a current density of 0.5 A g^{-1}. Figure 6e shows the relationship between the energy density and power density of the G electrode through Ragone plots that can be calculated from the GCD profiles.[9] The maximum energy density of the sample at 80 °C has a value of 7.16 W h kg^{-1}, higher than that of the sample at 25 and 50 °C, with values of 6.14 and 6.88 W h kg^{-1}, respectively, at the power density of 250 W kg^{-1}. At a power density of 5000 W kg^{-1}, the G electrode measured at three different temperatures of 25, 50, and 80 °C has values of 4.16, 4.21, and 4.44 W h kg^{-1}, respectively.

Similar to the graphene electrode, the C_{NPs} electrode was also investigated for electrochemical properties through CV, EIS, and GCD profiles. At different temperatures (25, 50, and 80 °C), the material's voltage changes linearly in the negative direction from −0.5 to +0.5 V and vice versa. As shown in Figure 7a−c, the CV curves of C_{NPs} at different scan rates and different temperatures have similar shapes and gradually become smaller when changing the scan speed from 200 to 5 mV. At high temperatures, the electrolyte gradually becomes unstable, causing evaporation, which directly affects the charge−discharge process at the electrode−electrolyte interface and also causes fluctuations at the outer Helmholtz plane

https://doi.org/10.1021/acsomega.3c08537
ACS Omega 2024, 9, 22543−22556

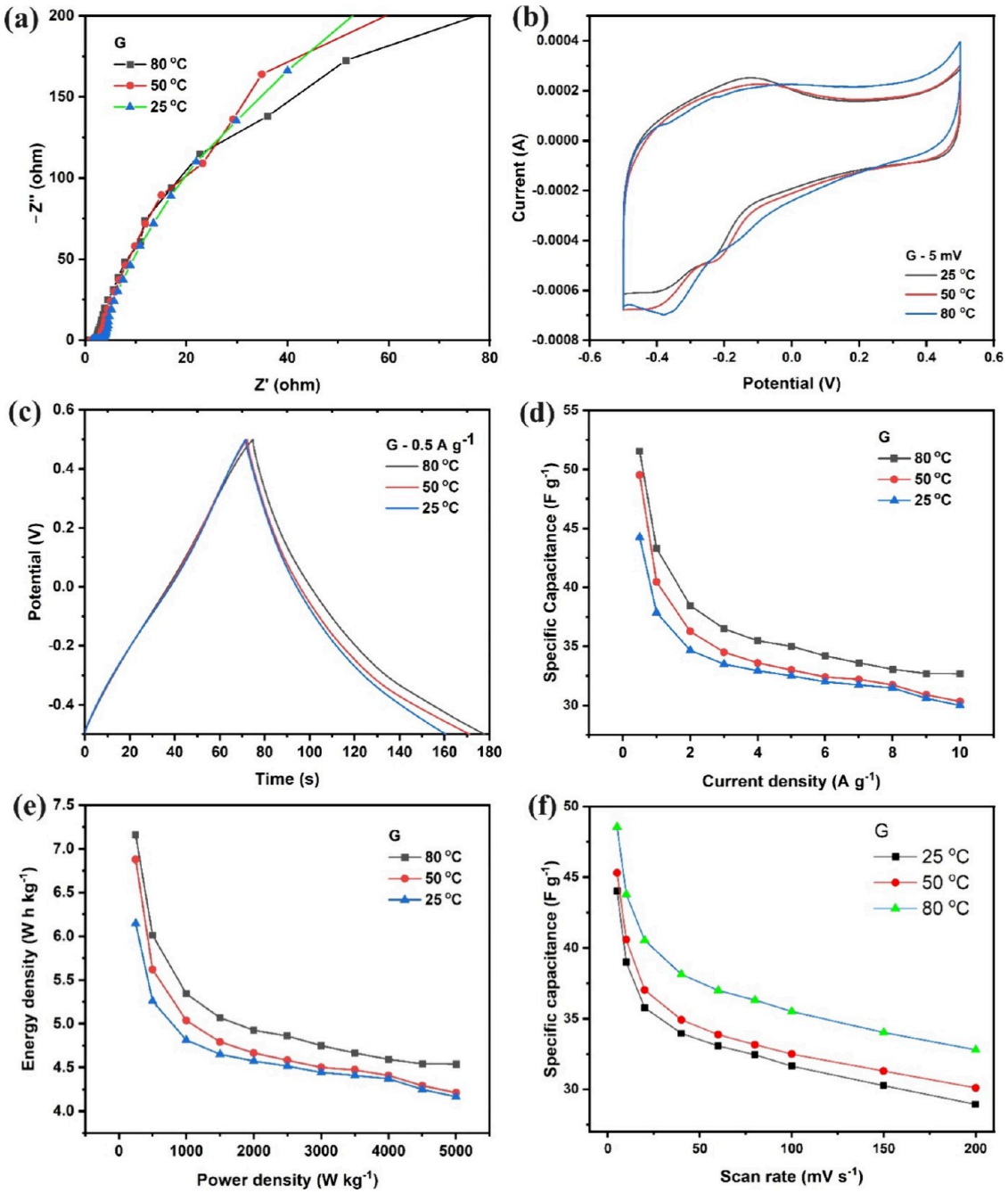

Figure 6. Electrochemical studies of a three-electrode system for G electrodes: (a) EIS plots, (b) CV comparison curves at three temperatures at 5 mV s^{-1}, (c) GCD comparison curves at three temperatures at 0.5 A g^{-1}, (d) specific capacitance following different current densities, (e) Ragone plots, and (f) specific capacitance following different scan rates.

layer. Therefore, the CV curves at high temperatures in Figure 7b,c have a certain deformation. The GCD curves in Figure 7d−f illustrate shapes close to triangles indicating efficient ion transport via stable double-layer capacitor behavior.[38,39] In addition, at different current densities from 10 to 0.5 A g^{-1}, the GCD curves showed linearity with stable discharge reversibility of the C_{NPs} electrode. Moreover, the Coulombic efficiency of the C_{NPs} working electrode is shown in Table 1 in comparison with the G electrode, which is related to the electrochemical capability via the charge−discharge process. Supercapacitors made of carbon materials store energy based on the charge−discharge process through the surface reaction of the electrode material which forms a double layer on the porous electrode. As a result, supercapacitors offer a higher power density per unit space than batteries do. The charge on the electrodes of a typical supercapacitor always grows (or declines) linearly, resulting in voltage rises (or falls) during the charge and discharge process. This is another electrochemical feature that sets supercapacitors apart from batteries. Figure 7a−c illustrates how the supercapacitor's cyclic voltammetry (CV) curve stays essentially rectangular during the charge and discharge operation (Figure 7d−f), while the current is nearly constant. Furthermore, the galvanostatic charge−discharge (GCD) curves often have a consistent slope.

Figure 8a shows the EIS results of the C_{NPs} electrode in the range of 100 mHz to 100 kHz with an amplitude of 5 mV. The

https://doi.org/10.1021/acsomega.3c08537
ACS Omega 2024, 9, 22543−22556

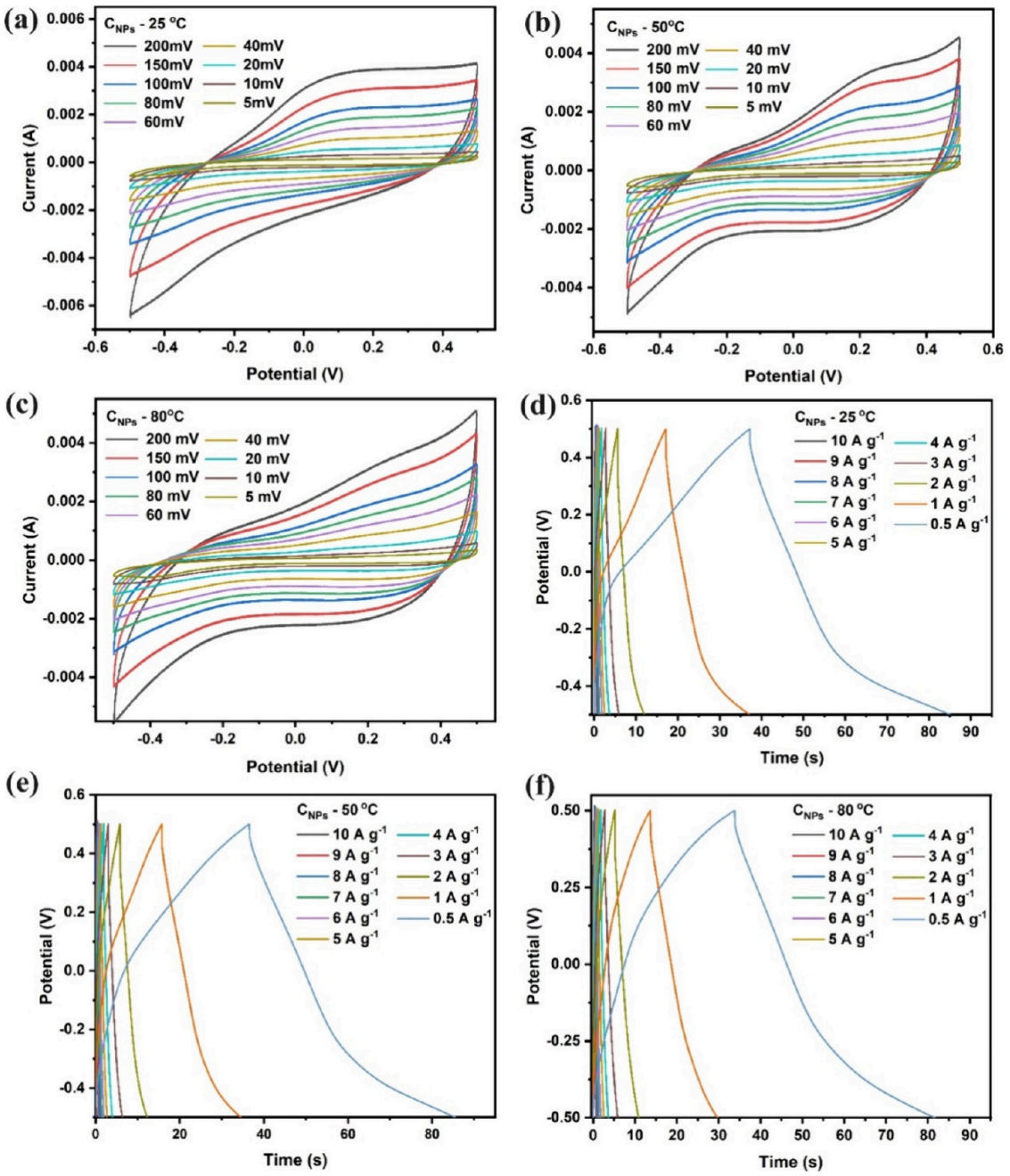

Figure 7. Electrochemical studies of a three-electrode system for C_{NPs} electrodes: (a−c) CV curves and (d−f) GCD curves at 25, 50, and 80 °C, respectively.

equivalent series resistances of the samples measured at different temperatures of 25, 50, and 80 °C are 3.2, 3.1, and 4.06 Ω, respectively. Additionally, Figure S1b of the fitted EIS plot based on the Randles circuit depicts an equivalent electrical circuit with an impedance Warburg element and an active electrolyte resistance *R* connected to a double-layer capacitance *C*. Figure 8b shows the CV curves of C_{NPs} samples with an electrolyte of 1 M Na_2SO_4 at a scan rate of 5 mV s^{-1}at different temperatures. The CV curves of C_{NPs} in the electrolyte at different temperatures work quite well without too much variation. When the temperature rises to a peak of 80 °C, C_{NPs} shows signs of mild deformation. Furthermore, this result illustrates that the CV curves for all these cells show a shape that closely resembles a rectangle, showing EDLC behavior with fairly good capacitive behavior and a fast current response. Through Figure 8b,c, it can be clearly seen that the CV curves and GCD curves of the C_{NPs} sample at different temperatures almost coincide with each other at the same scan rate of 5 mV and a current density of 0.5 A g^{-1}. This also proves that the C_{NPs} electrode is durable at high temperatures. The specific capacitance is calculated based on the CV curve and is shown in the graph in Figure 8c. At 200 mV s^{-1}, the specific capacitance has values of 10.58, 8.77, and 9.76 F g^{-1} at different temperatures of 25, 50, and 80 °C, respectively. When the scan rate is gradually decreased, the specific capacitance gradually increases: 23.14, 23.96, and 24.98 F g^{-1} at 5 mV s^{-1}, respectively. Figure 8d shows the electrochemical performance of the C_{NPs} electrode at different temperatures (25, 50, and 80

https://doi.org/10.1021/acsomega.3c08537
ACS Omega 2024, 9, 22543−22556

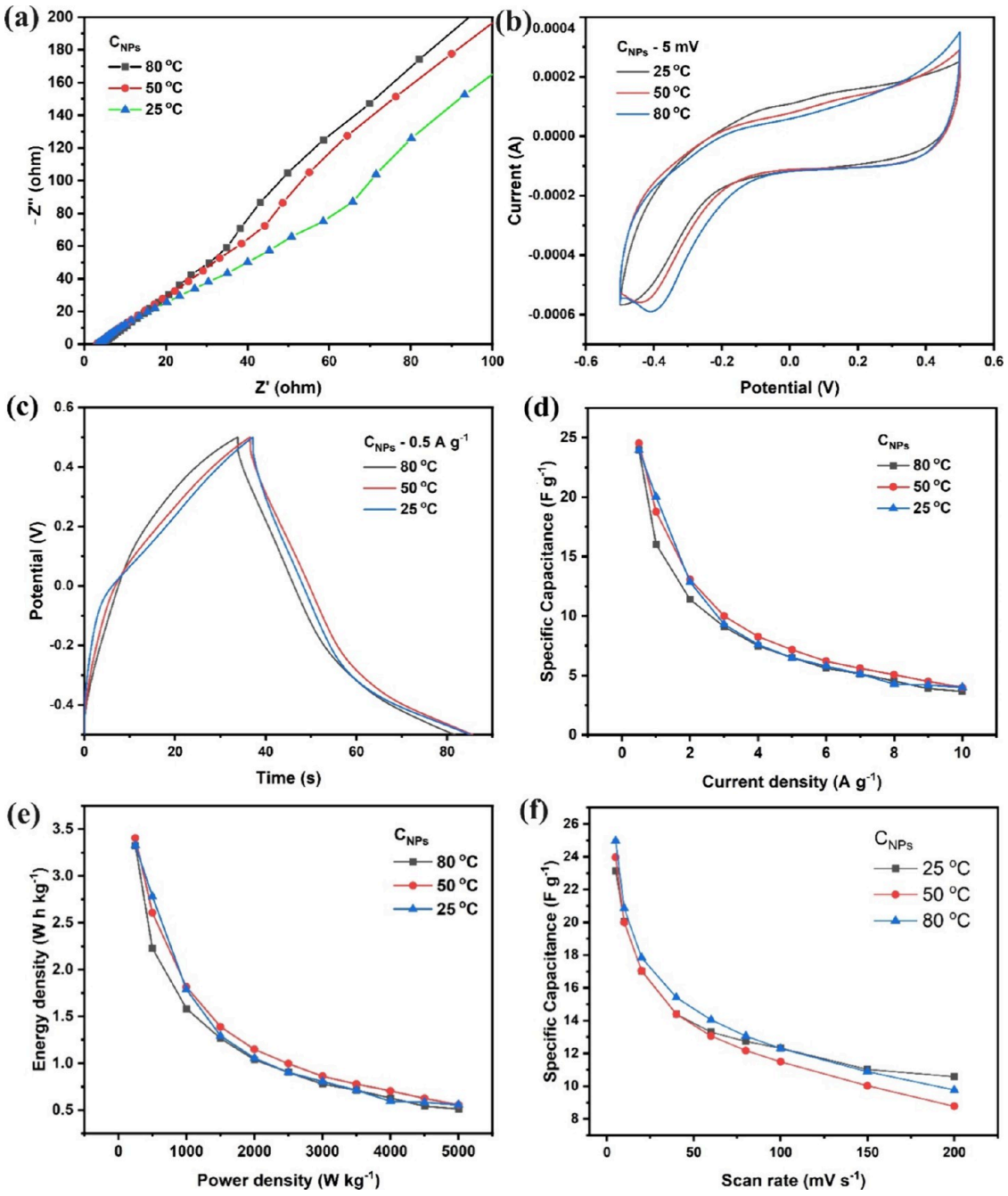

Figure 8. Electrochemical studies of a three-electrode system for the C_{NPs} electrode: (a) EIS plots, (b) CV comparison curves at three temperatures at 5 mV s^{-1}, (c) GCD comparison curve at three temperatures at 0.5 A g^{-1}, (d) specific capacitance following different current densities, (e) Ragone plots, and (f) specific capacitance following different scan rates.

°C), which obtained the maximum specific capacitance of 23.95, 24.52, and 23.93 F g^{-1}, respectively, at a current density of 0.5 A g^{-1}. Figure 8e shows the relationship between the energy density and electrical density of the electrode containing C_{NPs} through Ragone plots that can be calculated from the GCD profiles. The maximum energy density of the sample at 50 °C has a value of 3.4 W h kg^{-1} higher than the sample at 25 and 80 °C, which have a value of 3.33 W h kg^{-1} at a power density of 250 W kg^{-1}. At a power density of 5000 W kg^{-1}, samples at different temperatures have negligible and approximately equal changes in power density values. Moreover, Figure 8f illustrates the specific capacitance of the C_{NPs} electrode at various different CV scan rates, which point out similar capacitive values in comparison with GCD curves. More clearly, Table 2 illustrates the comparison of electrochemical studies of graphene nanosheets and carbon nanoparticles with previous reports, which provide a general view of the promising recycling techniques for zinc−carbon batteries in this research.

3.2.2. Electrochemical Studies of Devices. To better understand the electrochemical performance of graphene nanosheets and carbon nanoparticles, symmetric solid-state supercapacitors were assembled to characterize. A combination of electrodes separated by an electrolyte and separator is called an electric double-layer capacitor. The current collector's surface is covered in a powdered form of graphene or carbon

https://doi.org/10.1021/acsomega.3c08537
ACS Omega 2024, 9, 22543−22556

Table 2. Electrochemical Studies of Carbon Materials in This Report in Comparison with Previous Report

material	method to preparation	electrolyte	specific capacitance (F g^{-1})	energy density	ref.
CNT	CVD	KOH activation	53.6 F g^{-1} at 50 mA g^{-1}	N/A	40
activated carbon	spray coating	PVA/ADP	39.8 F g^{-1} at 0.12 mA cm^{-2}	205 μW h^2 cm^{-2}	41
banana fiber-derived activated carbon	pyrolysis	1 M Na_2SO_4	74 F g^{-1} at 0.5 A g^{-1}	N/A	42
graphene nanosheets _ H^+	plasma exfoliation	1 M NaCl	67.1 F g^{-1} at 5 mV s^{-1}	N/A	43
graphene nanosheets _ Na^+			21.6 1 F g^{-1} at 5 mV s^{-1}		
graphite			11.4 1 F g^{-1} at 5 mV s^{-1}		
surface-exfoliated graphite pencil electrodes	surface exfoliation	0.1 M H_2SO_4	53.6 mF cm^{-2} at 0.1 mA cm^{-2}	7.4 μW h cm^{-2}	44
expanded graphite foil	electrochemical expansion	1 M H_2SO_4	65 mF cm^{-2} at 20 mA cm^{-2}	N/A	45
graphene nanosheets	electrochemical exfoliation	1 M Na_2SO_4	44.25 F g^{-1} at 0.5 A g^{-1}	6.15 W h kg^{-1}	**This work**
carbon nanoparticles	treatment	1 M Na_2SO_4	23.95 F g^{-1} at 0.5 A g^{-1}	3.33 W h kg^{-1}	**This work**

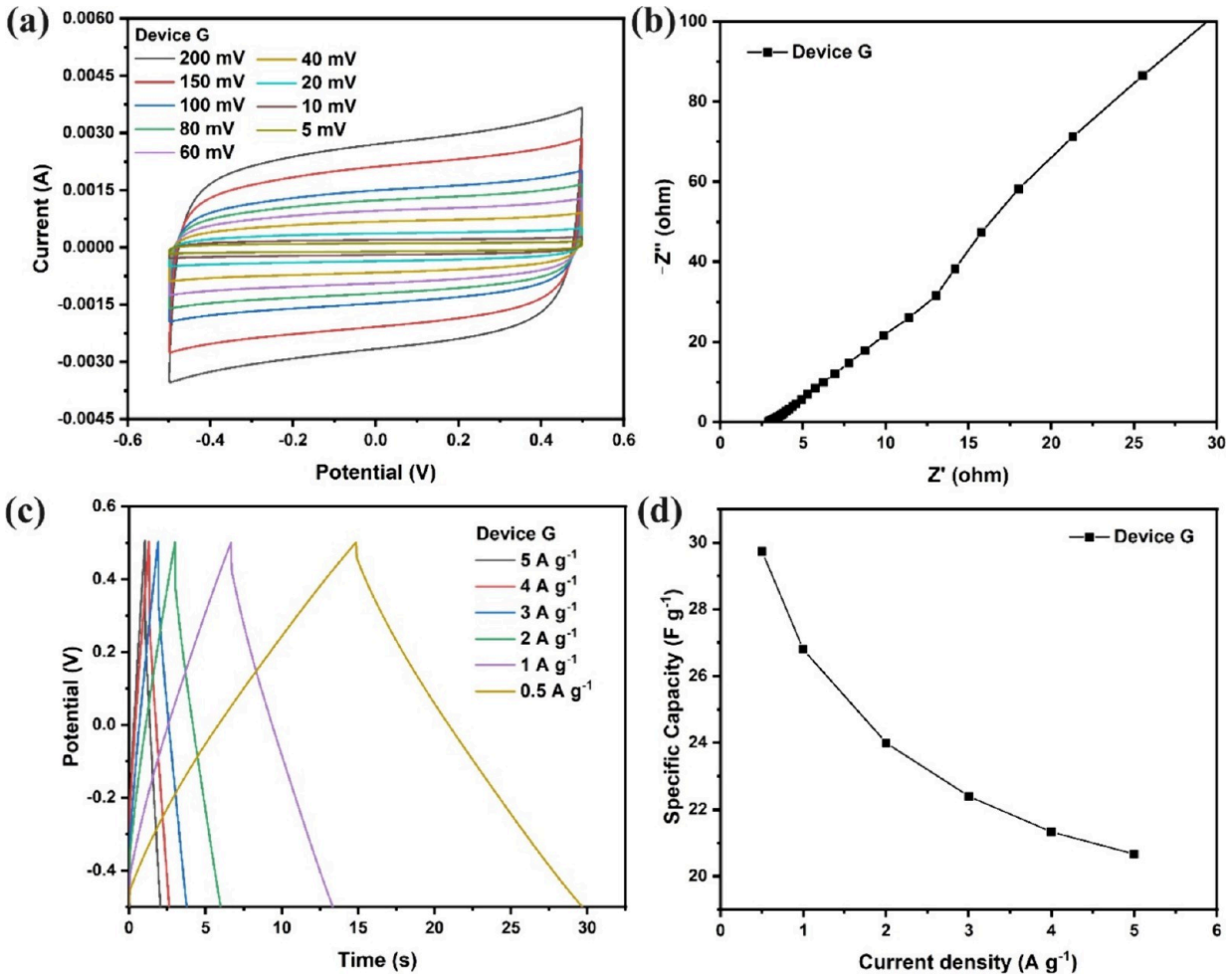

Figure 9. Electrochemical studies of devices G: (a) CV curves, (b) EIS plots, (c) GCD curves, and (d) specific capacitance following different current densities.

nanoparticles to obtain the supercapacitor electrodes. At the interface, where the electrolyte makes contact with the electrode layer, an electric double layer is created. For experimental purposes, Figure S2 shows the electric double layer of the supercapacitor in this report and the following circuit system: the anode capacitor (C_A) and cathode capacitor (C_C), as well as the electrode resistance (R_1 and R_2), internal resistance of the electrolyte and separator (R_{SE}), and insulation resistance (R_{i1} and R_{i2}). Anions and cations migrate to the positive and negative electrodes during the charge process and return to the electrolyte layer during the discharge process.

Figure 9a describes the CV curves of the symmetrical solid-state supercapacitor-based graphene nanosheet electrodes (device G) at different scan rates from 200 to 5 mV, and the striped rectangle in the range from −0.5 to 0.5 V shows relatively excellent conductivity and charging characteristics with good discharge. Figure 9b shows the EIS results of device G in the range of 100 mHz to 100 kHz with an amplitude of 5 mV. The equivalent series resistance of device G has a low value of 2.9 Ω, which indicates the good conductivity of the electrode/electrolyte interface. Moreover, the GCD curves in Figure 9c confirm the CV results. The specific capacitance calculated from the GCD line has the highest capacitance at

https://doi.org/10.1021/acsomega.3c08537
ACS Omega 2024, 9, 22543−22556

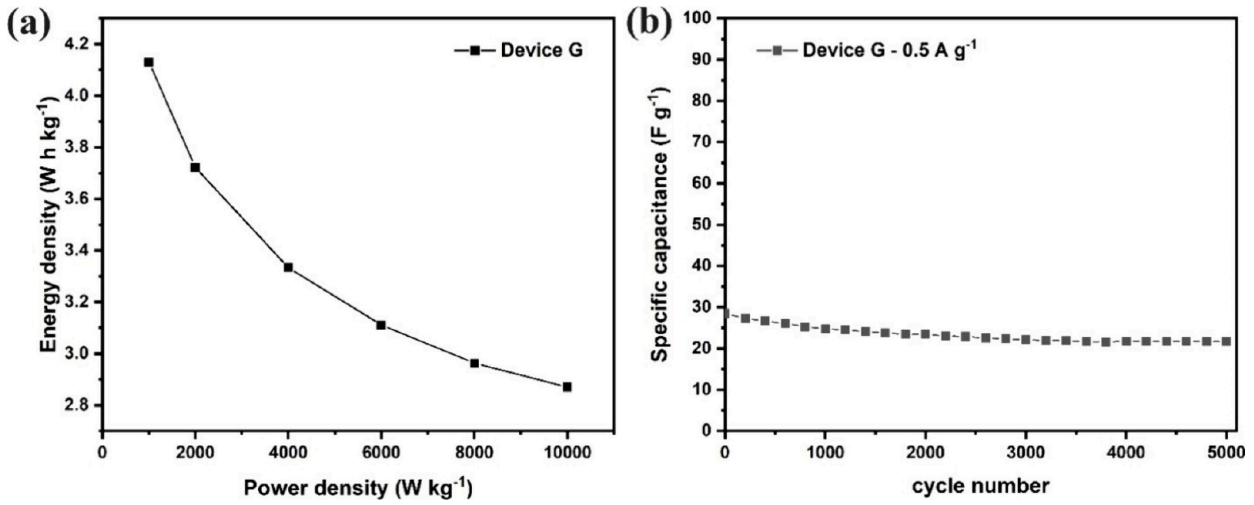

Figure 10. Electrochemical studies of devices G: (a) Ragone plot, (b) stability based on charge−discharge at 0.5 A g^{-1}.

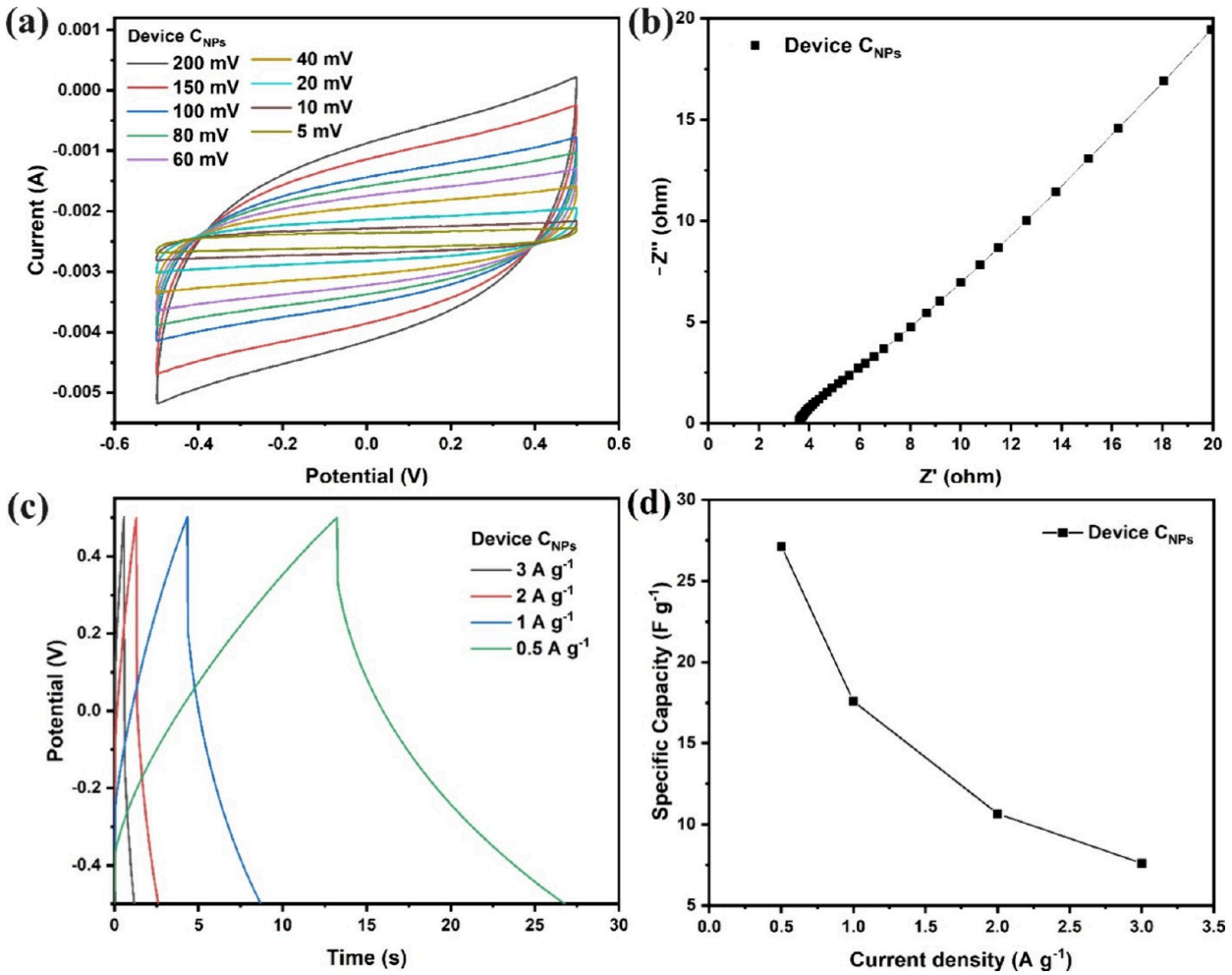

Figure 11. Electrochemical studies of devices: (a) CV curves, (b) EIS plots, (c) GCD curves, and (d) specific capacitance following different current densities.

0.5 A g^{-1} with a value of 30 F g^{-1} and the lowest capacitance at 5 A g^{-1} with a value of 21 F g^{-1} (Figure 9d). Figure 10a shows the relationship between the energy density and power density of device G through the Ragone diagram that can be calculated from the GCD profiles. The maximum energy density of device G has a value of 4.13 W h kg^{-1} at a power density of 1000 W kg^{-1}, and the minimum energy density has a value of 2.87 W h kg^{-1} at a power density of 10,000 W kg^{-1}. To investigate the stability of device G, it was studied by charge−discharge at a current density of 0.5 A g^{-1} after 5000 cycles to reflect the energy storage performance durability (Figure 10b). Here, after 5000 cycles, the specific capacitance of device G retains

https://doi.org/10.1021/acsomega.3c08537
ACS Omega 2024, 9, 22543−22556

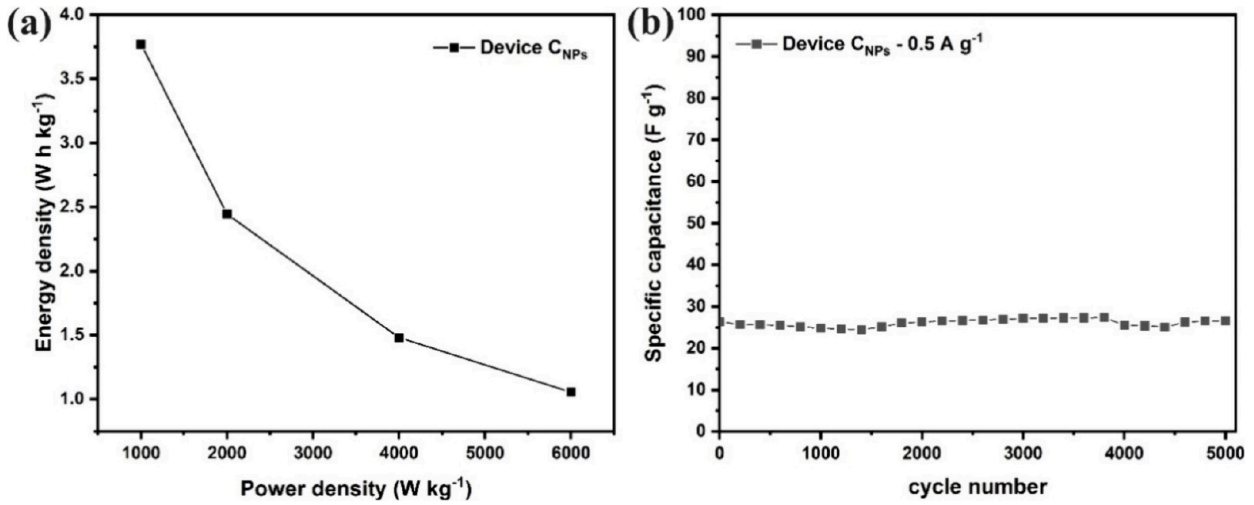

Figure 12. Electrochemical studies of devices C_{NPs}: (a) Ragone plot and (b) stability based on charge−discharge at 0.5 A g^{-1}.

about 73.33% (~22 F g^{-1}) of the initial capacitance. In summary, symmetrical solid-state supercapacitor devices using a graphene nanosheet material, which is recycled from spent zinc−carbon batteries, can be considered good candidates for solid-state supercapacitors.

Carbon nanoparticle-based solid-state supercapacitor devices, with the name device CNPs, are used in the construction of supercapacitor electrodes concurrently with the study of graphene nanosheets. The concept of recycling nearly all of the carbon material in a zinc−carbon battery is shown by these results, which are explored and displayed below. Figure 11a depicts the CV curves of the device C_{NPs} with different scan rates from 200 to 5 mV in the range from −0.5 to +0.5 V, showing an almost rectangular shape. The equivalent series resistance (ESR) of the EIS measurement for device C_{NPs} in Figure 11b provides a value of 3.6 Ω. Figure 11c shows the GCD curve of device C_{NPs} with a shape close to an isosceles triangle and a fast charge−discharge time. The specific capacitance of device C_{NPs} is calculated according to the GCD curve, which shows the highest specific capacitance of 27 F g^{-1} at 0.5 A g^{-1} and still obtains 6 F g^{-1} at the lowest current densities of 3 A g^{-1}. The dependence of specific capacitance on scanning density is shown in Figure 11d, and it can be seen that the capacitance increases with decreasing scanning density from 3 to 0.5 A g^{-1}, indicating good electrochemical properties. Figure 12a shows the dependence of energy density and power capacity calculated according to the GCD curve of the device C_{NPs}. The maximum energy density of the device C_{NPs} obtains a good value of 3.77 W h kg^{-1} at a power density of 1000 W kg^{-1}, and it is still 1.06 W h kg^{-1} at 6000 W kg^{-1}. Figure 12b illustrates the cyclic stability of the device C_{NPs} during 5000 cycles of charge−discharge at 0.5 A g^{-1}, which reflects the energy storage durability. After 5000 cycles, the capacitance at loop 5000 has a value of ~27 F g^{-1} (100% retention), which shows the very stable supercapacitor devices.

4. CONCLUSIONS

In summary, carbon nanoparticles and graphene nanosheet materials have been synthesized by using simple methods to obtain relatively good materials. The best thing about this report is the almost comprehensive and easy battery recycling method for carbon−zinc batteries. Through surveys at different temperatures, it has been shown that the material is relatively stable at all temperatures; there is not much change here. For supercapacitor applications, both graphene nanosheets and carbon nanoparticles have been shown to be stable over long periods, with graphene nanosheets (device G) having a specific capacitance of 22 F g^{-1} after 5000 cycles (85% reduction compared to the initial cycle), while the carbon nanoparticle material (device C_{NPs}) has a specific capacitance of 27 F g^{-1} after 5000 cycles (100% retention) and is relatively stable compared to the first cycle. Utilizing all of the materials in used batteries has contributed to reducing environmental pollution from carbon batteries.

■ ASSOCIATED CONTENT

Supporting Information

The Supporting Information is available free of charge at https://pubs.acs.org/doi/10.1021/acsomega.3c08537.

Nyquist plots and fitting results with the Randles equivalent circuit model at 25 °C of graphene nanosheets and carbon nanoparticle samples for a three-electrode system and general structure for an electric double-layer capacitor (PDF)

■ AUTHOR INFORMATION

Corresponding Authors

Nghia Trong Nguyen − *School of Chemical Engineering, Hanoi University of Science and Technology, Hanoi 100000, Vietnam*; Email: nghia.nguyentrong@hust.edu.vn

Thi Viet Bac Phung − *Center for Environmental Intelligence and College of Engineering and Computer Science, Vin University, Hanoi 100000, Vietnam*; orcid.org/0000-0001-7717-2538; Email: bac.ptv@vinuni.edu.vn

Authors

Thuy Trang T. Vuong − *Center for Environmental Intelligence and College of Engineering and Computer Science, Vin University, Hanoi 100000, Vietnam*

Phi Long Nguyen − *Center for Environmental Intelligence and College of Engineering and Computer Science, Vin University, Hanoi 100000, Vietnam*

Phuoc-Anh Le − *Center for Environmental Intelligence and College of Engineering and Computer Science, Vin University, Hanoi 100000, Vietnam; Institute of Chemistry, Vietnam*

https://doi.org/10.1021/acsomega.3c08537
ACS Omega 2024, 9, 22543−22556

Academy of Science and Technology, Hanoi 100000, Vietnam; orcid.org/0000-0003-4549-4166

Complete contact information is available at: https://pubs.acs.org/10.1021/acsomega.3c08537

Notes

The authors declare no competing financial interest.

■ ACKNOWLEDGMENTS

The authors acknowledge the support given by the VinUniversity, Vietnam (VinUniversity Seed Grant, no. VUNI.2223.FT09).

■ REFERENCES

(1) Olabi, A. G. Renewable energy and energy storage systems. *Energy* **2017**, *136*, 1−6.
(2) Sayed, E. T.; Olabi, A. G.; Alami, A. H.; Radwan, A.; Mdallal, A.; Rezk, A.; Abdelkareem, M. A. Renewable Energy and Energy Storage Systems. *Energies* **2023**, *16*, 1415.
(3) Hossain, E.; Faruque, H. M. R.; Sunny, M. S. H.; Mohammad, N.; Nawar, N. A Comprehensive Review on Energy Storage Systems: Types, Comparison, Current Scenario, Applications, Barriers, and Potential Solutions, Policies, and Future Prospects. *Energies* **2020**, *13*, 3651.
(4) Mahlia, T. M. I.; Saktisahdan, T. J.; Jannifar, A.; Hasan, M. H.; Matseelar, H. S. C. A review of available methods and development on energy storage; technology update. *Renewable and sustainable energy reviews* **2014**, *33*, 532−545.
(5) Ibrahim, H.; Ilinca, A.; Perron, J. Energy storage systems—Characteristics and comparisons. *Renew. Sustain. Energy Rev.* **2008**, *12* (5), 1221−1250.
(6) Olabi, A. G.; Abdelkareem, M. A. Energy storage systems towards 2050. *Energy* **2021**, *219*, No. 119634.
(7) Melchor-Martínez, E. M.; Macias-Garbett, R.; Malacara-Becerra, A.; Iqbal, H. M. N.; Sosa-Hernández, J. E.; Parra-Saldívar, R. Environmental impact of emerging contaminants from battery waste: A mini review. *Case Stud. Chem. Environ. Eng.* **2021**, *3*, No. 100104.
(8) Bro, P.; Levy, S. C. Batteries and the environment. *Stud. Environ. Sci.* **1994**, *59*, 131−162.
(9) Le, P. A.; Le, V. Q.; Nguyen, N. T.; Nguyen, V. T.; Thanh, D. V.; Phung, T. V. B. Multifunctional applications for waste zinc−carbon battery to synthesize carbon dots and symmetrical solid-state supercapacitors. *RSC Adv.* **2022**, *12* (17), 10608−10618.
(10) Toro, L.; Moscardini, E.; Baldassari, L.; Forte, F.; Falcone, I.; Coletta, J.; Toro, L. A Systematic Review of Battery Recycling Technologies: Advances, Challenges, and Future Prospects. *Energies* **2023**, *16* (18), 6571.
(11) Bernardes, A. M.; Espinosa, D. C. R.; Tenório, J. A. S. Recycling of batteries: a review of current processes and technologies. *J. Power Sources* **2004**, *130*, 291−298.
(12) Ippolito, N. M.; Belardi, G.; Medici, F.; Piga, L. Utilization of automotive shredder residues in a thermal process for recovery of manganese and zinc from zinc−carbon and alkaline spent batteries. *Waste management* **2016**, *51*, 182−189.
(13) Belardi, G.; Lavecchia, R.; Medici, F.; Piga, L.; Zuorro, A. A new thermal process for the recovery of metals from zinc-carbon and alkaline spent batteries. *American Journal of Applied Sciences* **2014**, *11* (9), 1566.
(14) Gabal, M. A.; Luhaibi, R. S. A.; Angari, Y. M. A. Recycling spent zinc−carbon batteries through synthesizing nano-crystalline Mn−Zn ferrites. *Powder Technol.* **2014**, *258*, 32−37.
(15) Salam, M. A.; Gabal, M. A.; Angari, Y. M. A. The recycle of spent Zn−C batteries and the synthesis of magnetic nanocomposite from graphene nanosheets and ferrite and its application for environmental remediation. *J. Mater. Res. Technol.* **2022**, *18*, 4267−4276.
(16) Petranikova, M.; Ebin, B.; Mikhailova, M.; Steenari, B. M.; Ekberg, C. Investigation of the effects of thermal treatment on the leachability of Zn and Mn from discarded alkaline and ZnC batteries. *Journal of Cleaner Production* **2018**, *170*, 1195−1205.
(17) Belardi, G.; Medici, F.; Piga, L. Influence of gaseous atmosphere during a thermal process for recovery of manganese and zinc from spent batteries. *J. Power Sources* **2014**, *248*, 1290−1298.
(18) Liu, S.; Yin, Y.; Hui, K. N.; Hui, K. N.; Lee, S. C.; Jun, S. C. High-Performance Flexible Quasi-Solid-State Supercapacitors Realized by Molybdenum Dioxide@Nitrogen-Doped Carbon and Copper Cobalt Sulfide Tubular Nanostructures. *Adv. Sci.* **2018**, *5*, No. 1800733.
(19) Miller, E. E.; Hua, Y.; Tezel, F. H. Materials for energy storage: Review of electrode materials and methods of increasing capacitance for supercapacitors. *J. Energy Storage* **2018**, *20*, 30−40.
(20) Forouzandeh, P.; Kumaravel, V.; Pillai, S. C. Electrode materials for supercapacitors: a review of recent advances. *Catalysts* **2020**, *10* (9), 969.
(21) Kumar, N.; Kim, S. B.; Lee, S. Y.; Park, S. J. Recent advanced supercapacitor: a review of storage mechanisms, electrode materials, modification, and perspectives. *Nanomaterials* **2022**, *12* (20), 3708.
(22) Poonam Sharma, K.; Arora, A.; Tripathi, S. K. Review of supercapacitors: Materials and devices. *J. Energy Storage* **2019**, *21*, 801−825.
(23) Afif, A.; Rahman, S. M.; Tasfiah Azad, A.; Zaini, J.; Islan, M. A.; Azad, A. K. Advanced materials and technologies for hybrid supercapacitors for energy storage−A review. *J. Energy Storage* **2019**, *25*, No. 100852.
(24) Liu, S.; Kang, L.; Jun, S. C. Challenges and Strategies toward Cathode Materials for Rechargeable Potassium-Ion Batteries. *Adv. Mater.* **2021**, *33*, No. 2004689.
(25) Li, Q.; Deng, R.; Chen, Y.; Gong, J.; Wang, P.; Zheng, Q.; Huo, Y.; Xie, F.; Wei, X.; Yang, C.; Lin, D. Homologous Heterostructured NiS/NiS2@C Hollow Ultrathin Microspheres with Interfacial Electron Redistribution for High-Performance Sodium Storage. *Small* **2023**, *19*, No. 2303642.
(26) González, A.; Goikolea, E.; Barrena, J. A.; Mysyk, R. Review on supercapacitors: Technologies and materials. *Renewable and sustainable energy reviews* **2016**, *58*, 1189−1206.
(27) Le, P. A.; Nguyen, V. T.; Yen, P. J.; Tseng, T. Y.; Wei, K. H. A new redox phloroglucinol additive incorporated gel polymer electrolyte for flexible symmetrical solid-state supercapacitors. *Sustainable Energy Fuels* **2019**, *3*, 1536−1544.
(28) Ouyang, W.; Zeng, D.; Yu, X.; Xie, F.; Zhang, W.; Chen, J.; Yan, J.; Xie, F.; Wang, L.; Meng, H.; Yuan, D. Exploring the active sites of nitrogen-doped graphene as catalysts for the oxygen reduction reaction. *International journal of hydrogen energy* **2014**, *39* (28), 15996−16005.
(29) Shanmugam, M.; Durai, M.; Sengottaiyan, C.; Ahn, Y. H. Effective chemical vapor deposition and characterization of N-doped graphene for high electrochemical performance. *J. Nanosci. Nanotechnol.* **2021**, *21* (6), 3183−3191.
(30) Malard, L. M.; Pimenta, M. A.; Dresselhaus, G.; Dresselhaus, M. S. Raman spectroscopy in graphene. *Physics reports* **2009**, *473* (5−6), 51−87.
(31) Khamlich, S.; Abdullaeva, Z.; Kennedy, J. V.; Maaza, M. High performance symmetric supercapacitor based on zinc hydroxychloride nanosheets and 3D graphene-nickel foam composite. *Appl. Surf. Sci.* **2017**, *405*, 329−336.
(32) Li, J.; Liu, W.; Xiao, D.; Wang, X. Oxygen-rich hierarchical porous carbon made from pomelo peel fiber as electrode material for supercapacitor. *Appl. Surf. Sci.* **2017**, *416*, 918−924.
(33) Hamouda, H. A.; Cui, S.; Dai, X.; Xiao, L.; Xie, X.; Peng, H.; Ma, G. Synthesis of porous carbon material based on biomass derived from hibiscus sabdariffa fruits as active electrodes for high-performance symmetric supercapacitors. *RSC Adv.* **2021**, *11* (1), 354−363.

(34) Du, C. F.; Zhao, X.; Wang, Z.; Yu, H.; Ye, Q. Recent advanced on the MXene−organic hybrids: Design, synthesis, and their applications. *Nanomaterials* **2021**, *11* (1), 166.
(35) Yuan, G.; Liang, Y.; Hu, H.; Li, H.; Xiao, Y.; Dong, H.; Liu, Y.; Zheng, M. Extraordinary thickness-independent electrochemical energy storage enabled by cross-linked microporous carbon nanosheets. *ACS Appl. Mater. Interfaces* **2019**, *11* (30), 26946−26955.
(36) Zhao, G.; Li, Y.; Zhu, G.; Lu, T.; Pan, L. Biomass-based N, P, and S self-doped porous carbon for high-performance supercapacitors. *ACS Sustain. Chem. Eng.* **2019**, *7* (14), 12052−12060.
(37) Wu, D.; Cheng, J.; Wang, T.; Liu, P.; Yang, L.; Jia, D. A novel porous N-and S-self-doped carbon derived from chinese rice wine lees as high-performance electrode materials in a supercapacitor. *ACS Sustainable Chem. Eng.* **2019**, *7* (14), 12138−12147.
(38) Yang, S.; Wang, S.; Liu, X.; Li, L. Biomass derived interconnected hierarchical micro-meso-macro-porous carbon with ultrahigh capacitance for supercapacitors. *Carbon* **2019**, *147*, 540−549.
(39) Wang, Q.; Yan, J.; Wei, T.; Feng, J.; Ren, Y.; Fan, Z.; Zhang, M.; Jing, X. Two-dimensional mesoporous carbon sheet-like framework material for high-rate supercapacitors. *Carbon* **2013**, *60*, 481−487.
(40) Xu, B.; Wu, F.; Su, Y.; Cao, G.; Chen, S.; Zhou, Z.; Yang, Y. Competitive effect of KOH activation on the electrochemical performances of carbon nanotubes for EDLC: Balance between porosity and conductivity. *Electrochim. Acta* **2008**, *53* (26), 7730−7735.
(41) Yong, S.; Owen, J.; Beeby, S. Solid-State Supercapacitor Fabricated in a Single Woven Textile Layer for E-Textiles Applications. *Adv. Eng. Mater.* **2018**, *20* (5), 1700860.
(42) Subramanian, V.; Luo, C.; Stephan, A. M.; Nahm, K. S.; Thomas, S.; Wei, B. Supercapacitors from activated carbon derived from banana fibers. *J. Phys. Chem. C* **2007**, *111* (20), 7527−7531.
(43) Yen, P. J.; Sahoo, S. K.; Chiang, Y. C.; Huang, S. Y.; Wu, C. W.; Hsu, Y. C.; Wei, K. H. Using different ions to tune graphene stack structures from sheet-to onion-like during plasma exfoliation, with supercapacitor applications. *Nanoscale Res. Lett.* **2019**, *14*, 1−11.
(44) AbdelHamid, A. A.; Elgamouz, A.; Kawde, A. N. Controlled electrochemical surface exfoliation of graphite pencil electrodes for high-performance supercapacitors. *RSC Adv.* **2023**, *13* (31), 21300−21312.
(45) Li, H. Y.; Yu, Y.; Liu, L.; Liu, L.; Wu, Y. One-step electrochemically expanded graphite foil for flexible all-solid supercapacitor with high rate performance. *Electrochim. Acta* **2017**, *228*, 553−561.

https://doi.org/10.1021/acsomega.3c08537
ACS Omega 2024, 9, 22543−22556